Article

Experimental Analysis of Ultrasonic Multiple Scattering Attenuation through the Air with Fine Dust

Ukyong Woo [1], Hajin Choi [1,*] and Homin Song [2,*]

1   School of Architecture, Soongsil University, Seoul 06978, Korea; ukdragon@soongsil.ac.kr
2   Department of Mechanical Engineering-Engineering Mechanics, Michigan Technological University, Houghton, MI 49931, USA
*   Correspondence: hjchoi@ssu.ac.kr (H.C.); shm3313@gmail.com (H.S.)

Abstract: In this study, we experimentally evaluated the application of multiple scattering theory for measuring ultrasonic attenuation. Based on the independent approximation theory, the method adopted for calculating the attenuation of coherent waves through air with fine dust is discussed. To obtain a scattering wavefield, a unique ultrasonic scattering hardware was developed, and signal processing schemes were suggested. Four cases of standard particle doses (0, 0.004, 0.008, and 0.012 g) were investigated inside a chamber. The results obtained from the experiments demonstrate that the proposed signal processing approach successfully calculates the scattering attenuation, which correlates well with the applied doses of fine dust. In addition, we discuss the irregular shape and composition of fine dust relative to the scattering cross-section.

1. Introduction

Fine dust particles in the air, such as particulate matter, have been a serious societal challenge worldwide [1–3]. Shridhar et al. investigated the composite of dust in India [1] while Nowak et al. and Jim and Chen discussed a removal methodology in China and the United States [2,3]. Airborne fine dust is a critical environmental issue and a potential threat to human health [4]. In particular, the heavy density of fine dust in the air causes secondary indoor air pollution in urban areas because people avoid natural ventilation via fresh air.

Therefore, the accurate measurement of fine dust concentration is essential for human health. Currently, the proposed techniques for measuring the concentration of fine dust include the beta ray, gravimetric, light scattering, and semiconductor-based gas sensor methods [5]. The beta line and gravimetric methods, which have relatively high accuracy, are not suitable for real-time data collection because they require the collection time of fine dust for a certain period [6,7]. The most widely used light scattering method is based on the light source phenomenon, where laser is scattered proportionally to the concentration of fine dust [8]. The gas sensor is based on the contraction and expansion effect, as well as the change in electrical resistance triggered by adsorption and desorption when fine dust contacts the surface of the semiconductor. Although light scattering and gas sensors that provide fast data at relatively low prices have been widely applied in the field, they are susceptible to environmental factors such as relative humidity; hence the need for additional calibration procedures [9–11].

Mechanical waves can be applied to the measurement of dust particles, where the wave propagation is less susceptible to changes in relative humidity. Ultrasound has been employed to estimate dust concentration in various industrial fields. Fu et al. evaluated the aluminum dust concentration in a spherical vessel [12] while Kazys et al. monitored the dust concentration in a powder classifier [13]. A recent study conducted by the authors

proposed a fine dust measurement method based on the independent scattering approximation theory and verified its effectiveness via numerical simulation [14]. The number of fine dust particles per unit area, called the number density, is directly computed by the scattering wavefield without additional calibration. The proposed theory numerically evaluated that the attenuation of coherent waves over the frequency corresponds well with the number density under a low volume fraction of the fine dust in air (below 2%).

In this study, the ultrasonic multiple scattering method for estimating the number density was experimentally verified. A series of ultrasonic experiments were performed with and without a controlled environment. The number density of fine dust particles was calculated using the measured ultrasonic data based on the independent scattering approximation theory. The signal processing procedure was also suggested by considering a three-dimensional wave propagation, such as geometric spreading. The unique contributions of this study are summarized as follows: (1) it provides the first experimental validation for the measurement of fine dust in air using mechanical wave scattering, (2) it develops an ultrasonic multiple scattering hardware that measures the attenuation of propagating waves in linear space, and (3) it develops a signal processing procedure that calculates ultrasonic scattering attenuation triggered by fine dust in air using the proposed ultrasonic scattering method.

The structure of this article includes a theoretical background on multiple scattering of acoustic waves in randomly distributed particles through the medium in Section 2, signal processing in Section 3, experimental details in Section 4, and experimental results and discussion in Sections 5 and 6, respectively. Additionally, we discuss the air quality index for understanding the gap between the measured number density and mass concentration of fine dust in air.

2. Scattering Attenuation Defined by Independent Scattering Approximation

When acoustic waves are propagated through a disordered medium similar to the air with fine dust, multiple scattering occurs and the amplitude of the waves is attenuated. The attenuation triggered by scattering has been studied via statistical approximation. As the distance between the source and receiver is comparably longer than the scattering mean free path (l_S), considering the contribution of infinite multiple scattering, it is a challenge to accurately express the solution for the wave motion. However, statistical approaches, such as ensemble averaging, can be taken. Ensemble averaging reduces the effect of incoherent scattering triggered by the reverberation between scatterers [15]. The ensemble averaged Green's solution <G> in the frequency (ω) -wave number (k) domain is expressed as:

$$\langle G(\omega, \boldsymbol{k}) \rangle = \frac{1}{k_0{}^2(\omega) - \Sigma(\omega, \boldsymbol{k}) - k^2} \tag{1}$$

where k_0 and Σ represent the wave number in the homogeneous background medium and the self-energy that represents the contribution of ultrasonic multiple scattering, respectively.

Independent scattering approximation (ISA) modifies the self-energy as being independent of $\boldsymbol{k}$ for a certain range of frequencies, provided the sizes of the scatterers are not too large compared to the wavelength and are completely uncorrelated [16]. The ISA concept introduces the effective wave number (k_e) in a quasi-homogeneous medium (effective medium) [17–21] as:

$$k_e{}^2(\omega) = k_0{}^2(\omega) - \Sigma(\omega) \tag{2}$$

The effective medium is based on the hypothesis that every element in the composite acts as an isolated element embedded in a homogenous medium with effective composite properties. As the theory provides a simple approach to determining effective properties, the approach has been successfully adopted in many fluid and solid cases [22–24].

In this study, the attenuation of the effective medium is considered as the scattering attenuation of coherent waves through air with fine dust. The attenuation is defined by the imaginary part of the effective wave number given by:

$$\alpha = 2\text{Im}(k_e) \tag{3}$$

In the ISA, the attenuation also exhibits the following relationship:

$$\alpha = n\sigma_t \tag{4}$$

where n and σ_t represent the number density and scattering cross-section of one scatterer, respectively. Therefore, the defined scattering attenuation correlates with the amount of fine dust in air. Further details on the scattering attenuation in the experiment are described in the following section.

3. Signal Processing

In this study, the signal processing method is suggested for calculating the scattering attenuation of coherent waves through air with fine dust. Figure 1 presents an overview of the signal processing method used to compute the scattering attenuation from coherent wave responses. First, ensemble averaging is performed over M realizations.

$$\langle s(x_i, t) \rangle = \frac{1}{N} \sum_{m=1}^{M} s_m(x_i, t), \tag{5}$$

where $\langle s(x_i, t) \rangle$ and $s_m(x_i, t)$ are the ensemble-averaged coherent wave response at the ith receiver position and m^{th} single-realization response at the receiver position, respectively. Then, the ensemble-averaged response $\langle S(x_i, t) \rangle$ is converted from the time domain to the frequency domain using Fourier transform, which is expressed as:

$$\langle S(x_i, f) \rangle = \int_{-\infty}^{\infty} \langle s(x_i, t) \rangle e^{-j2\pi ft} dt, \tag{6}$$

where $\langle S(x_i, f) \rangle$ is the ensemble-averaged response in the frequency domain. We assume that the magnitude spectra in the frequency domain $A(x_i, f)$ can be expressed in the following form:

$$A(x_i, f) = \frac{1}{x_i} A_0(f) e^{-\alpha(f)x_i}, \tag{7}$$

where $A_0(f)$ and $\alpha(f)$ represent the ensemble-averaged wave magnitude at the source position and frequency-dependent scattering attenuation, respectively. Furthermore, $A(x_i, f)$ is expressed as:

$$A(x_i, f) = \sqrt{(\text{Re}[\langle S(x_i, f) \rangle])^2 + (\text{Im}[\langle S(x_i, f) \rangle])^2}, \tag{8}$$

where Re[.] and Im[.] represent the real and imaginary parts of values in the bracket, respectively. Then, the scattering attenuation $\alpha(f)$ is computed by considering the slope parameter of the least-squares fit of $\ln[x_i A(x_i, f)]$ given by:

$$\ln[x_i A(x_i, f)] = \ln[A_0(f)] - \alpha(f)x_i. \tag{9}$$

$$s_m(x_i, t)$$

$$\downarrow$$

Ensemble averaging

$$\downarrow$$

$$\langle s(x_i, t) \rangle$$

$$\downarrow$$

Fourier transform

$$\downarrow$$

$$\langle S(x_i, f) \rangle$$

$$\downarrow$$

Magnitude spectra

$$\downarrow$$

$$A(x_i, f)$$

$$\downarrow$$

Linear regression using the assumed model

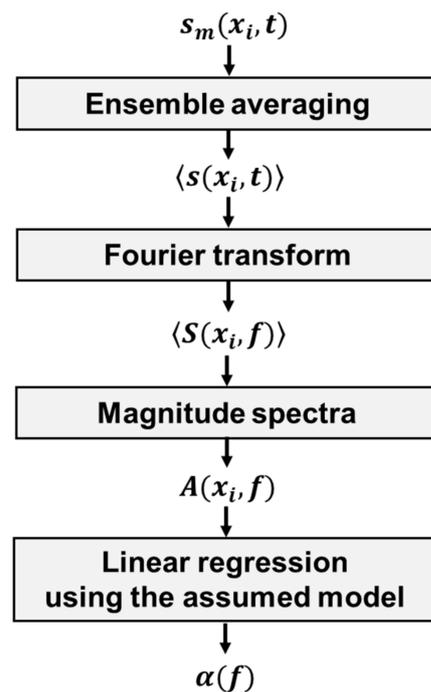$$\downarrow$$

$$\alpha(f)$$

Figure 1. Conceptual illustration of signal processing for scattering attenuation.

Note that the assumed model in Equation (7) considers the geometric spreading with the $1/x_i$ term. Therefore, the amplitude decay triggered by the geometric spreading in the three-dimensional space is compensated for in the computed scattering attenuation.

4. Experimental Details

4.1. Ultrasonic Scattering Hardware

In the experiment, the frequency bands generated by the transducer are practically limited, unlike in numerical studies. In addition, the corresponding scattering regime is based on the wavelength of acoustic waves. The size of fine dust compared to the applied wavelength (λ) is calculated as the size parameter approximation (x), which is expressed as:

$$x = \frac{2\pi a}{\lambda} \tag{10}$$

where a is the radius of the scatterer. The size effect is categorized by the scatterings of Mie and Rayleigh when the size parameter is approximately one and smaller than one, respectively. The ultrasonic transducer was carefully selected with a fine dust diameter of 10 μm (PM10). The applied transducers have a center frequency of 5 MHz and wavelength of approximately 68 μm in air (with an acoustic wave velocity of 343 m/s at 20 °C). The size parameter approximation is approximately 0.46, which is considered under Rayleigh scattering with an acceptable ISA range.

To measure ultrasonic multiple scattering through air with fine dust, an air-coupled testing scheme is designed based on the suggested attenuation measurement. Figure 2a presents a schematic illustration of the experimental set-up. The experimental hardware includes a pair of air-coupled transducers (Ultran NCT5-D13), power amplification (E&I 210L), waveform generator (Keysight 33500B), and digitizer (NI-PXIe-1071). To obtain the attenuation of the coherent wave, the distance between the transmitter and receiver is continuously and accurately increased using a DC-micromotor (Fraubaber 3242024CR). The DC-micromotor is carefully controlled by a pulse, where 10 pulses are required for a linear motion in a 0.2 μm distance (encoder: 1000 pulse and gear ratio: 43:1). Practically, 1500 pulses are selected and the corresponding moving distance is 300 μm. The developed controller system is presented in Figure 2b, which shows the control button and monitor.

(a)

(b)
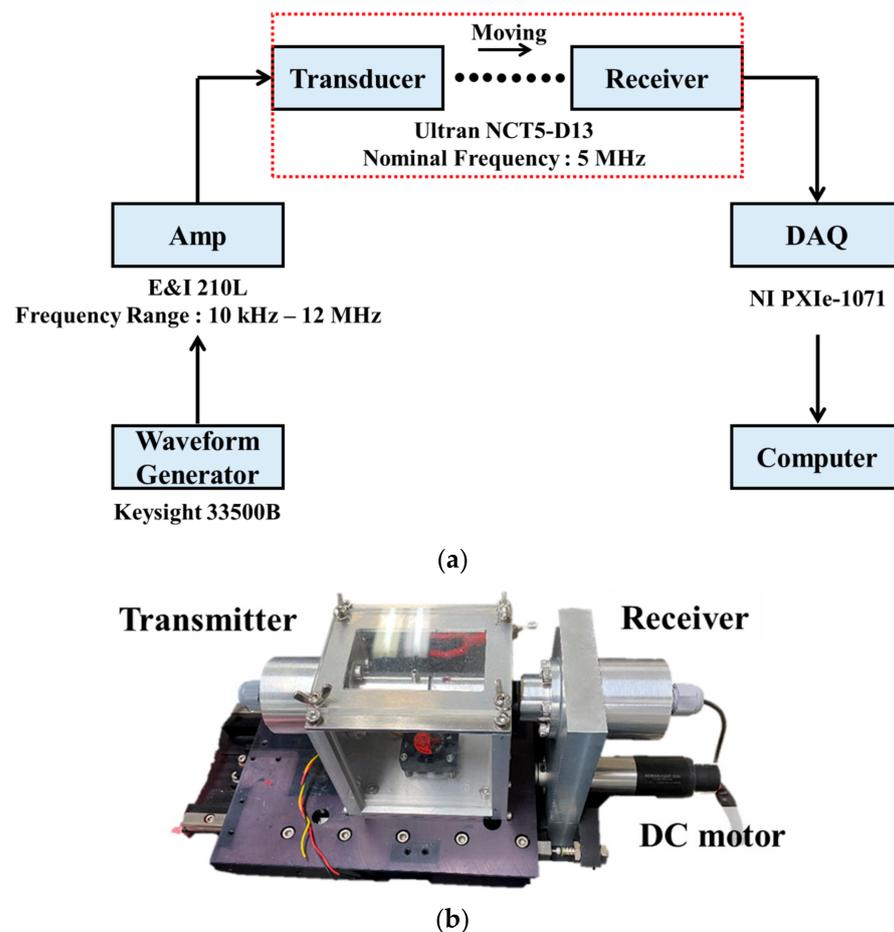
Figure 2. Ultrasonic multiple scattering hardware: (**a**) schematic illustration of the experimental setup, and (**b**) picture of moving platform using DC-micromotor.

4.2. Fine Dust Materials

Standard particles (ISO 12103-1, A1 ultrafine test dust) were adopted in this multiple scattering experiment. The standard particles were composed of silicon, aluminum, iron, calcium, potassium, sodium magnesium, and titanium, and the density of the composite was 500 kg/m^3. To determine the shape of the particles, micro-scale images for a scoop of the particles were captured using a scanning electron microscope (Zeiss Gemini 300). It was observed that a surface coating procedure with magnetron sputtering was required to prevent image distortion caused by charged electrons. Secondary electron imaging was performed to obtain surface information. As shown in Figure 3, although the nominal diameter of the standard particles is less than 10 μm; the shape is irregular. The irregularities possibly affect the scattering cross-section, which is conventionally assumed to have a circular shape with a constant diameter. Further details on the influence of the shape are discussed in Section 6.

4.3. Experimental Procedure

Using the developed hardware, several ultrasonic multiple scattering experiments were performed. First, the experiment was conducted inside a chamber (400 mm × 400 mm × 400 mm). As shown in Figure 4, the chamber was made of transparent acrylic plates. Inside the chamber, four fans (5000 rpm) were positioned for circulating the fine dust during the measurement. In addition, a conventionally available environmental meter (K-weather IAQ-Station-LTE) was adopted to measure the relative humidity and temperature during the experiment.
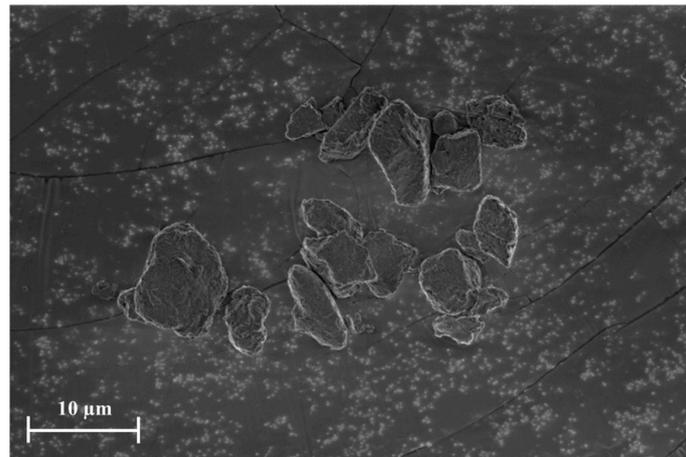
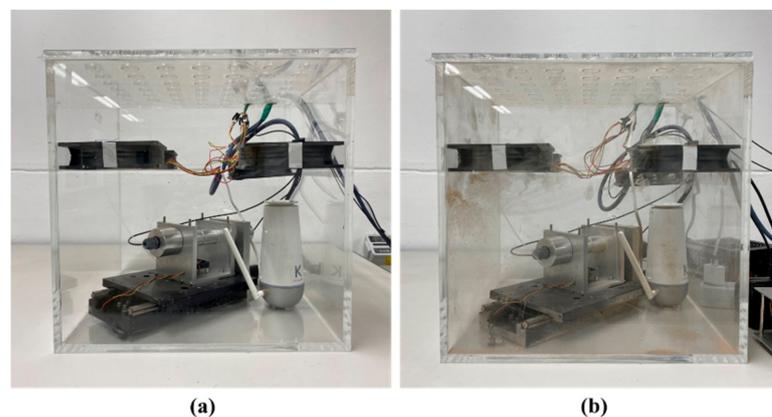**Figure 3.** Scanning electron microscope (SEM) image of standard particles.

Figure 4. Photograph of the experimental setup: (**a**) without fine dust, and (**b**) with fine dust (0.012 g).

The measurements were carried out without fine dust, and three cases with different doses (0, 0.004, 0.008, and 0.012 g) were evaluated. The standard particles were carefully weighed using a micro-scale. After pouring the fine dust into the chamber, the fans were switched on and the air quality immediately dropped. The environmental meter confirmed that the applied mass concentration and relative humidity were maintained during the measurement. From the transmitter, five cycles of the torn burst signal (center frequency of 5 MHz) were excited with an amplification of 40 dB. Then, the measured waveform was digitized with a 60 MHz sampling rate and 1500 time points. To eliminate low-frequency noise from the environment, a high-pass filter was applied with a cut-off frequency of 1 MHz. Time averaging was adopted 1000 times at each measurement to remove random electrical noise. The process of data acquisition is presented as follows: (1) the ultrasonic wave was first measured at a 1.7 mm gap between the transmitter and receiver. (2) The receiver was moved away from the transmitter with an interval of 300 μm. At each interval, data acquisition was repeated 10 times for ensemble averaging. (3) The final length of wave travel was 5 mm, where a total of 120 different time series data were obtained per case of the experiment.

5. Experimental Results

In this section, we present the acoustic wave signals collected using the experimental setup, as well as the scattering attenuation computed for a range of standard particle doses.

5.1. Multiply Scattered Acoustic Waves

Figure 5 presents examples of the acoustic wave responses measured by the experimental setup described in Section 4. The total number of ensembles to obtain the ensemble-averaged response presented in Figure 5a is 10 ($M = 10$), and Figure 5b represents one of the 10 ensembles. The single-realization response (Figure 5b) exhibits noise-like incoherent wave components, as well as a coherent wave pulse that is the dominant component. The incoherent wave components might have been set up by the standard particles distributed in the air of the test chamber. In the ensemble-averaged response (Figure 5a), only the coherent pulse is significant. The incoherent wave components observed in the single-realization response (Figure 5b) are suppressed and negligible in the ensemble-averaged response (Figure 5a).
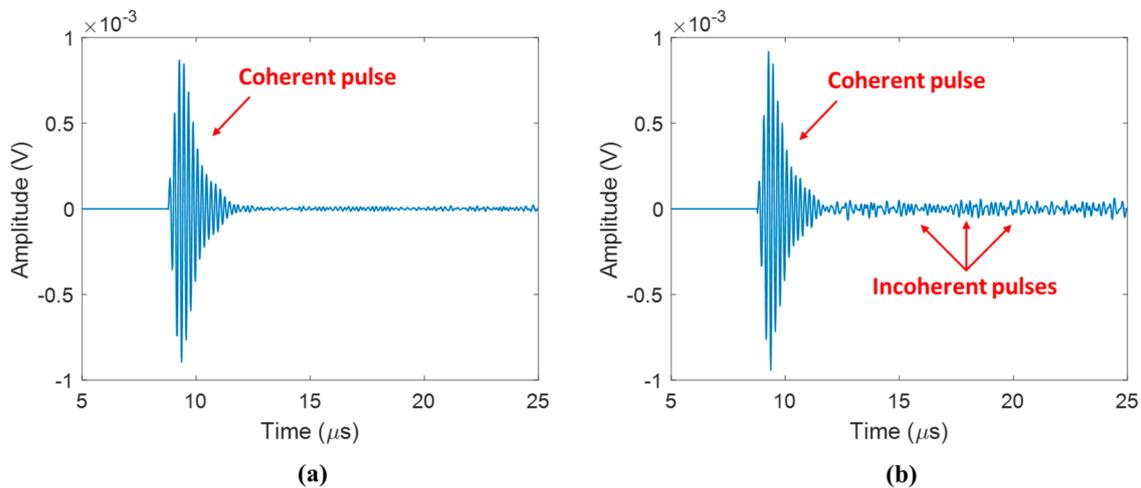

Figure 5. Examples of acoustic wave responses: (**a**) ensemble-averaged response $\langle s(x_1, t) \rangle$ and (**b**) single-realization response $s(x_1, t)$.

The time series of the ensemble-averaged response was transformed in the frequency domain, as illustrated in Figure 6. The center frequency is 4.8 MHz while the half-power bandwidth (*HPB*) ranges from 4.6 to 5.1 MHz. The attenuation of coherent waves over a 5 mm travel distance is clearly presented in the magnitude spectrum. The attenuation triggered by geometric spreading was compensated in the frequency domain. Then, using Equation (9), the scattering attenuation is calculated by considering the slope of the linear relationship between the travel distance x_i and the logarithm of the coherent wave's magnitude, $\ln[x_i A(x_i, f)]$. An example of the linear regression procedure is presented in Figure 7. Based on the coefficient of determination (R^2), the range that exhibits a strong positive relationship over 0.7 is between 4.4 and 5.2 MHz, which correlates well with the half-power bandwidth of the measured signals.
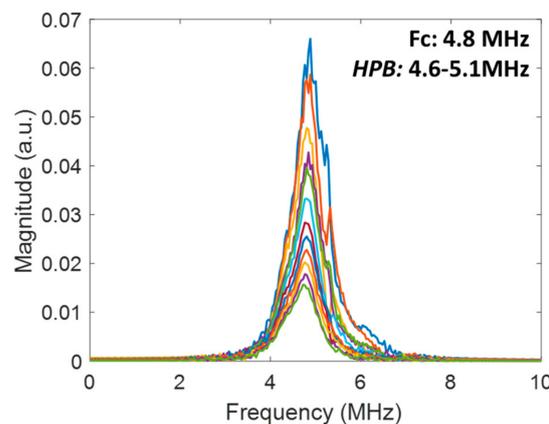

Figure 6. Acoustic wave responses $\langle S(x_i, f) \rangle$ in the frequency domain.
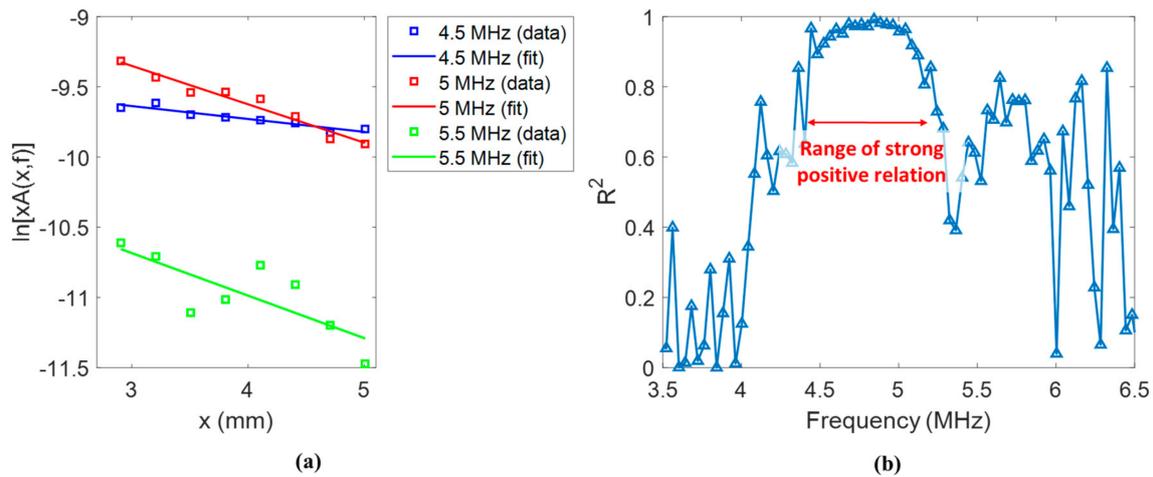
Figure 7. Example of linear regression using the assumed model: (**a**) least-squares fit, and (**b**) coefficient of determination.

5.2. Scattering Attenuation of Coherent Waves

The scattering attenuation computed using the signal processing method described in Section 3 is illustrated in Figure 8. In Figure 8, four cases of standard particle doses (0, 0.004, 0.008, and 0.012 g) are indicated. In all cases, the scattering attenuation increases as the frequency increases. The three particle dosage cases (0.004, 0.008, and 0.012 g) exhibit higher attenuation values than the zero-dosage case across the presented frequencies. The increase in attenuation is probably triggered by the particles dosed into the air in the test chamber, which interact with the incident acoustic waves. In the zero-dosage case, the attenuation exhibits non-trivial values above zero across frequencies, thereby indicating that other environmental factors, such as atmospheric moisture, and other dust particles in the air can contribute to the attenuation of coherent acoustic waves.
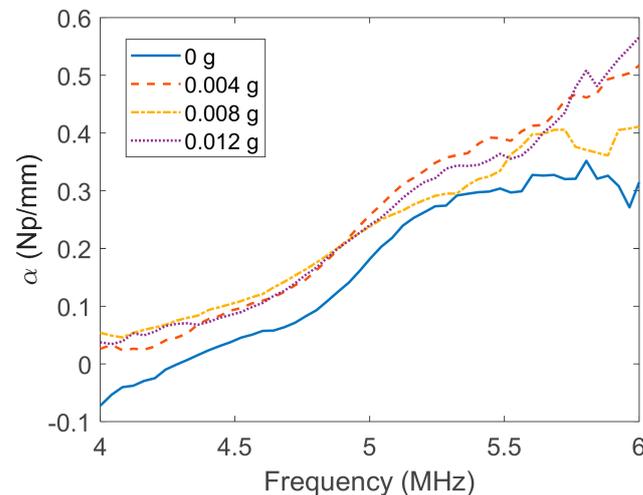

Figure 8. Coherent wave attenuation over the excitation frequency region.

To quantitatively investigate the effects of particle dosage on the coherent wave attenuation, attenuation values at several frequencies were obtained from Figure 8. Figure 9 presents the obtained values of attenuation at the frequencies (4–6 MHz with an increment of 0.5 MHz) across a range of standard particle doses. The presented results (Figures 8 and 9) indicate that the attenuation of coherent waves can be used to distinguish clean air and air from dust particles. In Figure 9a, although attenuation is observed to generally increase with the particle dosage increases, this increasing trend is not monotonic. For example, attenuation decreases from 0.004 to 0.008 g of particle dosage at 5.5 and

6 MHz. We inferred that the frequency range does not possess sufficient wave energy by the applied ultrasonic transducers, and that the corresponding linear regression is limited, as illustrated in Figure 7. Therefore, attenuation is averaged over the range of frequencies exhibiting a significant positive relationship with the regression in Figure 9b. Then, the increasing trend of the attenuation is clearly observed until the particle dosage of 0.008 g. In the 0.012 g dosage case, attenuation slightly decreases. This might indicate an experimental limitation because the amount of particles was not optimally distributed over the measurement, as presented in Figure 4b.
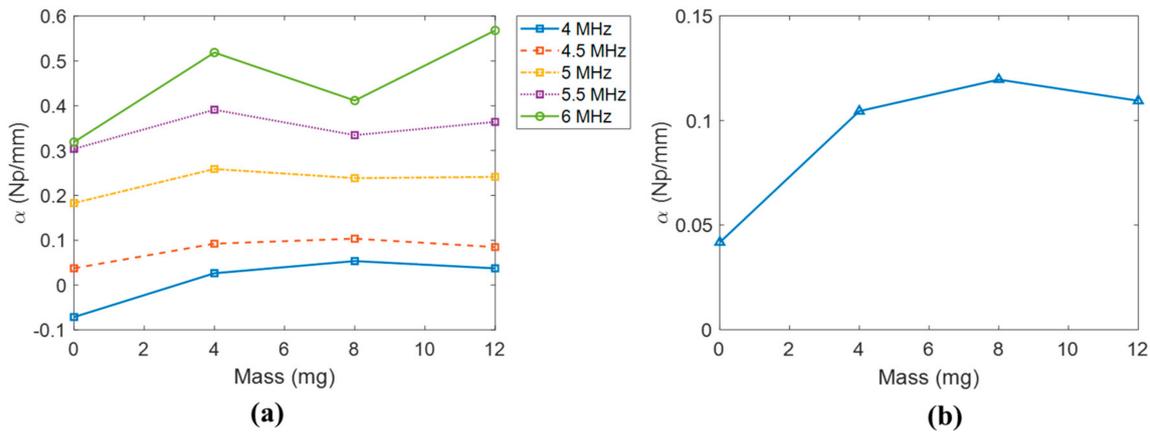

Figure 9. Coherent wave attenuation across a range of standard particle dosage: (**a**) at several frequencies, and (**b**) at averaged frequencies over a statistically valid region.

6. Discussion

Owing to the scattering attenuation obtained by the experiment, the number of fine dust particles per unit volume can be quantified with a scattering cross-section, based on Equation (4). For practical purposes, the scattering cross-section of fine dust is usually calculated assuming a spherical particle shape. However, the shape of fine dust particles is neither spherical nor regular. Therefore, we further investigated the shape effect with respect to the scattering cross-section to understand the variation range in the estimation of number density.

Analytical and numerical simulation studies were conducted to determine the scattering cross-section. The analytical solution of the scattering cross-section for a perfect circular particle can be calculated using Equation (11).

$$\sigma_t = 4a \frac{1}{ka} \left[\left| \frac{J_0'(ka)}{H_0^{(2)'}(ka)} \right|^2 + 2\sum \left| \frac{J_l'(ka)}{H_0^{(2)'}(ka)} \right|^2 \right], \tag{11}$$

where J_0 and $H_0^{(2)}$ are the Bessel functions of the first kind and Henkel function of the second kind, respectively. It is notable that the analytical expression correlates with the applied frequency range and size parameter in Equation (10). If the shape of the particle is not circular, the cross-section can be numerically calculated as:

$$\sigma_t = \int_0^{2\pi} |f(\varphi)|^2 d\varphi \tag{12}$$

where $f(\varphi)$ represents the scattered amplitude as a function of the azimuth (φ). The scattering cross-section is the total summation of the amplitude of the scattered wave, which can be measured by the sensors around the particle. A schematic illustration of the simulation is presented in Figure 10, where the scattered wave field is obtained by the sensors around the particle after the incident plane waves are propagated. The particle

shape was obtained from the scanning electron microscopy image of the actual fine dust sample, as illustrated in Figure 11a. The simulation was performed using a finite-difference time-domain (FDTD) simulation tool *k*-wave [25], and the simulation parameters used in this study are summarized in Table 1.
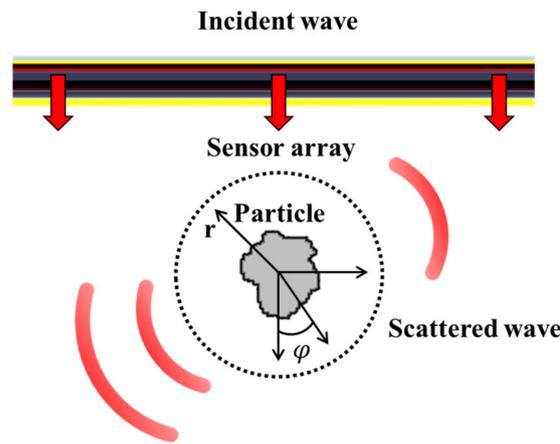

Figure 10. Schematic illustration of scattering cross-section calculation.
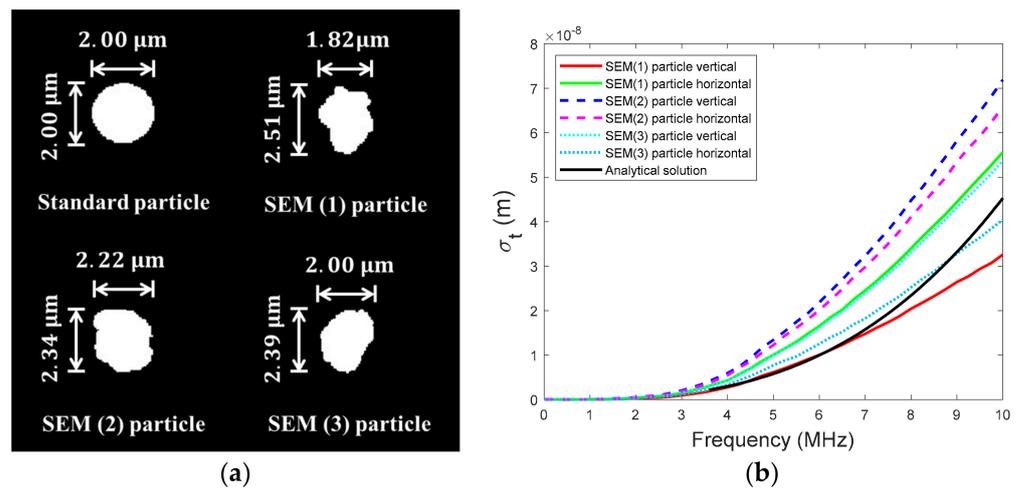

Figure 11. Analysis of scattering cross-section (**a**) particle shapes, (**b**) computed scattering cross-section.

Table 1. Summary of numerical simulation parameters.

Material Properties		
	Wave Speed (m/s)	**Mass Density (kg/m^3)**
Air	343	1.2754
Fine dust particle	343	500
Simulation parameters		
Number of grid points ($N_x \times N_y$)	1500×1500	
Grid spacing (dx and dy)	0.057 μm	
Time step (dt)	0.02 ns	
Time duration (T)	4 μs	
Number of sensing points	3676 (sensor array radius 37.05 μm)	
Sensor spacing along *y* axis	1.65 μm	
CFL condition	0.1	

In the numerical simulation, the scattering cross-sections of three different particle shapes were computed. A conventional desktop computer with a GPU (NVIDIA GeForce

RTX 2060 Super) was used for the simulation, and the average computation time per particle was approximately 16 h. To identify the directional effect, additional simulations were performed using 90° rotated particles (marked as vertical) relative to the incident wave. Figure 11b presents seven scattering cross-section values, including an analytical solution. The results obtained indicate that the analytical solution is within an acceptable range relative to SEM (1) vertical particle at the applied frequencies in this study. However, the scattering cross-section values from the other particles vary significantly, which possibly triggers erroneous numbers of fine dust particles. Interestingly, the direction of particles facing incident waves indicates a different scattering cross-section value. Therefore, quantifying the number of fine dust particles can be performed using a probability distribution with an uncertain range rather than suggesting exact numbers, which will be further investigated in future research.

7. Conclusions and Future Work

In this study, the experimental analysis of ultrasonic multiple scattering was performed to obtain the scattering attenuation triggered by fine dust particles in air. We proposed a signal processing approach based on an independent scattering approximation. Based on the results obtained, the following conclusions were drawn:

1. The developed ultrasonic scattering hardware enables the acquisition of meaningful signal data through air with fine dust (PM 10). The applied ultrasonic wavelength was approximately 68 μm in air and a total of 120 different time series data were obtained per case of the experiment.
2. The proposed signal processing approach (including ensemble averaging and Fourier analysis) enables the calculation of scattering attenuation, and the results obtained indicate a correlation between the scattering attenuation and the dosage of fine dust until 0.008 g.
3. The range of scattering cross-sections of actual fine dust particles is required to estimate the number of fine dust particles per unit volume. Numerical investigation presented the effect of irregular particle shape on the number density estimation.

In future work, the estimation of number density will be conducted to validate the proposed scattering attenuation approach.

Author Contributions: Conceptualization, H.S. and H.C.; Methodology, H.S. and H.C.; Investigation, U.W.; Data Curation, U.W.; Writing—Original Draft Preparation, H.S. and H.C.; Writing—Review and Editing, H.C.; Supervision, H.C.; Funding Acquisition, H.C. All authors have read and agreed to the published version of the manuscript.

Institutional Review Board Statement: Not applicable.

Informed Consent Statement: Not applicable.

Data Availability Statement: The data presented in this study are available on request from the corresponding author.

Conflicts of Interest: The authors declare no conflict of interest.

References

1. Shridhar, V.; Khillare, P.S.; Agarwal, T.; Ray, S. Metallic species in ambient particulate matter at rural and urban locations of Delhi. *J. Hazard. Mater.* **2010**, *175*, 600–607. [CrossRef] [PubMed]
2. Jim, C.Y.; Chen, W.Y. Assessing the ecosystem service of air pollutant removal by urban trees in Guangzhou (China). *J. Environ. Manag.* **2008**, *88*, 665–676. [CrossRef] [PubMed]
3. Nowak, D.J.; Crane, D.E.; Stevens, J.C. Air pollution removal by urban trees and shrubs in the United States. *Urban For. Urban Green.* **2006**, *4*, 115–123. [CrossRef]
4. Pope, C.A.; Dockery, D.W. Health effects of fine particulate air pollution: Lines that connect. *J. Air Waste Manag. Assoc.* **2006**, *56*, 709–742. [CrossRef] [PubMed]

5. Amaral, S.S.; de Carvalho, J.A.; Costa, M.A.M.; Pinheiro, C. An overview of particulate matter measurement instruments. *Atmosphere* **2015**, *6*, 1327–1345. [CrossRef]
6. Hauck, H.; Berner, A.; Gomiscek, B.; Stopper, S.; Puxbaum, H.; Kundi, M.; Preining, O. On the equivalence of gravimetric PM data with TEOM and beta-attenuation measurements. *J. Aerosol Sci.* **2004**, *35*, 1135–1149. [CrossRef]
7. Giechaskiel, B.; Maricq, M.; Ntziachristos, L.; Dardiotis, C.; Wang, X.; Axmann, H.; Bergmann, A.; Schindler, W. Review of motor vehicle particulate emissions sampling and measurement: From smoke and filter mass to particle number. *J. Aerosol Sci.* **2014**, *67*, 48–86. [CrossRef]
8. Chow, J.C.; Watson, J.G.; Park, K.; Lowenthal, D.H.; Robinson, N.F.; Park, K.; Maglian, K.A. Comparison of particle light scattering and fine particulate matter mass in central california. *J. Air Waste Manag. Assoc.* **2006**, *56*, 398–410. [CrossRef]
9. Lee, C.H.; Oh, S.N. Effect of Atmospheric Humidity on Fine Dust Measurement Using the Light Scattering Method. *J. Korean Soc. Hazard Mitig.* **2020**, *20*, 391–399. [CrossRef]
10. Kim, J.H.; Oh, J.; Choi, J.S.; Ahn, J.Y.; Yoon, G.H.; Park, J.S. A Study on the Correction of Optic Scattering PM2.5 by the Gravimetric Method. *J. Korean Soc. Urban Environ.* **2014**, *14*, 41–47.
11. Kim, S.J.; Kang, H.S.; Son, Y.S.; Yoon, S.L.; Kim, J.C.; Kim, G.S.; Kim, I.W. Compensation of Light Scattering Method for Real-Time Monitoring of Particulate Matters in Subway Stations. *J. Korean Soc. Atmos. Environ.* **2010**, *26*, 533–542. [CrossRef]
12. Fu, S.; Lou, W.; Wang, H.; Li, C.; Chen, Z.; Zhang, Y. Evaluating the effects of aluminum dust concentration on explosions in a 20 L spherical vessel using ultrasonic sensors. *Powder Technol.* **2020**, *367*, 809–819. [CrossRef]
13. Kazys, R.; Sliteris, R.; Mazeika, L.; Van den Abeele, L.; Nielsen, P.; Snellings, R. Ultrasonic monitoring of variations in dust concentration in a powder classifier. *Powder Technol.* **2020**, in press.
14. Song, H.M.; Woo, U.Y.; Choi, H.J. Numerical analysis of ultrasonic multiple scattering for fine dust number density estimation. *J. Appl. Sci.* **2020**. accpeted.
15. Tourin, A.; Derode, A.; Peyre, A.; Fink, M. Transport parameters for propagating an ultrasonic-pulsed wave in a multiple scattering medium. *J. Acoust. Soc. Am.* **2000**, *108*, 503–512. [CrossRef]
16. Tourin, A.; Fink, M.; Derode, A. Multiple scattering of sound. *Waves Random Media* **2000**, *10*, R31–R60. [CrossRef]
17. Lagendijk, A.; van Tiggelen, B.A. Resonant multiple scattering of light. *Phys. Rep.* **1996**, *29*, 143–215. [CrossRef]
18. Foldy, L.L. The multiple scattering of waves. I. General theory of isotropic scattering by randomly distributed scatterers. *Phys. Rev.* **1945**, *67*, 107–119. [CrossRef]
19. Lax, M. Multiple scattering of waves. II. The effective field in dense systems. *Phys. Rev.* **1952**, *85*, 621–629. [CrossRef]
20. Waterman, P.C.; Truell, R. Multiple scattering of waves. *J. Math. Phys.* **1961**, *2*, 512–537. [CrossRef]
21. Lloyd, P.; Berry, M.V. Wave propagation through an assembly of spheres: IV. Relationship between different multiple scattering theories. *Proc. Phys. Soc.* **1967**, *91*, 678–688. [CrossRef]
22. Kim, J.Y.; Ih, J.-G.; Lee, B.-H. Dispersion of elastic wave in random particulate composites. *J. Acoust. Soc. Am.* **1995**, *97*, 1380–1388. [CrossRef]
23. Choy, T.C. *Effective Medium theory: Principles and Applications*; Oxford University Press: New York, NY, USA, 2000; pp. 96–135.
24. Berge, P.A.; Bonner, B.P.; Berryman, J.G. Ultrasonic velocicty-porosity relationships for sandstone analogs made from fused glass beads. *Geophysics* **1995**, *60*, 108–119. [CrossRef]
25. Treeby, B.E.; Cox, B.T. k-Wave: MATLAB toolbox for the simulation and reconstruction of photoacoustic wave fields. *J. Biomed. Opt.* **2010**, *15*, 021314. [CrossRef] [PubMed]